Experimental Poststall Rotary Aerodynamic Coefficients for Airplane-like Configurations

M. H. Clarkson,* G.N. Malcolm,† and G. T. Chapman‡
NASA Ames Research Center, Moffett Field, Calif.

Military and civilian airplane losses caused by out-of-control spin motions are significant. Knowledge of rotary coefficients is necessary to understand the cause of spin entry and to devise proper recovery techniques. An exploratory wind-tunnel investigation has been conducted at Ames Research Center on simple airplane-like configurations on a rotary sting apparatus at rotation rates up to 10 rps. Rotary coefficients have been measured at unit Reynolds numbers from 2×10^6 m^{-1} to 24.6×10^6 m^{-1} and at angles of attack from 45° to 90°. Results show that the aerodynamic characteristics at steady spin rates are highly dependent on both spin rate and Reynolds number.

Nomenclature

A = body reference area, $\pi d^2/4$
b = wing span, 0.457 m (1.5 ft)
c_D = body drag force per unit length/qd
c'_N = body normal force per unit length/qd
C_R = moment about spin axis/qSb, positive clockwise (viewed from rear)
c'_y = body side force per unit length/qd
C_y = body side force/qA
d = diameter of center body, 0.0762 m (0.25 ft)
ℓ = length of nose section
M = freestream Mach number
N_1 = tangent ogive nose, see Fig. 4
q = freestream dynamic pressure
R_d = Reynolds number based on d
S = wing reference area, 0.0491 m^2 (0.5234 ft^2)
T_1 = aft body, circular cylinder tail section, see Fig. 4
T_2 = T_1 plus tail surfaces, see Fig. 4
U = freestream velocity
W = wing, see Fig. 4
x_n = distances, see Fig. 9
α_ℓ = local angle of attack, see Fig. 9
σ_f = angle between the freestream velocity vector and the body x axis
ψ = angle of roll about the body x axis
ω = angular velocity of the rotary sting
Ω = reduced spin rate, $\omega b/2U$

I. Introduction

SIGNIFICANT losses still occur to military and general aviation aircraft because of out-of-control motion associated with stall/spin problems at high angles of attack. To understand these phenomena better, governmental and industrial laboratories in the U.S. are conducting rigorous studies of the static and dynamic aerodynamic characteristics associated with airplane configurations at high angles of attack.

Tobak and Schiff[1] have shown, through an analytical formulation, that aerodynamic forces and moments which govern arbitrary aircraft motions can be determined experimentally from a specific set of wind-tunnel tests. These tests are performed with the model undergoing small-amplitude, forced oscillations about some mean angle of pitch and yaw and are carried out separately in the presence of a basic coning motion. The basic coning motion (without forced oscillation) can be obtained by attaching a model (at some fixed angle) to a rotary sting where the axis of rotation is aligned parallel to the wind-tunnel airstream and the nose of the model describes a circle about the freestream velocity vector. If the model is mounted on the sting with a six-component balance, the forces and moments so obtained represent the first terms in the formulation of Tobak and Schiff. Such rotary tests at constant angle of attack using six-component balances go back to 1933,[2] at least, but the data that are available, on modern configurations as well as old, have been limited to Reynolds numbers that are much too low to predict, confidently, full-scale behavior. Typically, Reynolds numbers based on maximum fuselage width R_d have ranged from 90,000 to 380,000.[3,4]

This investigation was exploratory in nature in that there were few specific goals dictating a rigorous schedule of model and tunnel conditions to be adhered to strictly for the duration of the experiment. Since the whole region of rotary testing at high Reynolds numbers is relatively unknown, the objectives of this test were to examine some possible pro-spin flow mechanisms and to evaluate their effects through a large Reynolds number range (R_d up to 1.5×10^6). Several nose and tail configurations were examined, as well as the effects with and without the wing. Three separate, but related, mechanisms for autorotation were selected for investigation (Fig. 1). The first one on the left illustrates a pair of asymmetric vortices which have been shown in static wind-tunnel tests, e.g., Keener and Chapman,[5] to occur on tangent ogive nose sections with and without cylindrical afterbodies at certain Mach number and Reynolds number conditions and angles of attack. The result of this flow asymmetry is a large side force and yawing moment which could be a potential source for autorotational motion. The second case is a non-circular cylinder which has been shown by Polhamus[6] to provide autorotative moments at certain Reynolds numbers. The particular configuration tested here, with a constant square cross section and rounded corners, was selected because extensive two-dimensional tests have been carried out by Polhamus[6] on this specific cross section. Testing the same cross section provides an opportunity to compare the present experimental rotary data with calculations based on previous static results. The third mechanism illustrated is for a tail configuration similar to a fighter airplane configuration that has been shown by Chambers et al.[3] to produce autorotative moments at low Reynolds numbers and Mach numbers.

Presented as Paper 75-171 at the AIAA 13th Aerospace Sciences Meeting, Pasadena, Calif., Jan. 20-22, 1975; submitted Feb. 28, 1975; revision received Jan. 20, 1976.

Index categories: Aircraft Aerodynamics (including Component Aerodynamics); Aircraft Handling, Stability, and Control; Aircraft Testing (including Component Wind Tunnel Testing).

*Professor of Engineering Science, University of Florida, Gainesville, Fla. Member AIAA.
†Research Scientist. Member AIAA.
‡Research Scientist, Chief, Aerodynamics Branch. Member AIAA.

II. Description of Experiment

A. Test Facilities and Models

The aerodynamic data presented here were obtained from wind-tunnel tests conducted in the 12-ft pressure wind tunnel at the Ames Research Center. This tunnel is a variable pressure, low-turbulence facility with a Mach number range of 0.1 to 0.98 and a unit Reynolds number capability of up to 29.5×10^6 m^{-1} (9×10^6 ft^{-1}) at $M=0.25$. The models were mounted on a rotary sting apparatus which originally was built for use with bodies of revolution in the Ames 6- by 6-foot wind tunnel.[7] The apparatus was modified for the present test and was mounted on the tunnel vertical strut in a conventional manner except for stiffening rods which were attached to both the vertical strut and the sting as shown in Fig. 2. The rate of rotation was varied from +600 rpm (clockwise) to -600 rpm by a variable displacement hydraulic pump and motor system.

The tests were carried out in two series. The first employed a single six-component internal strain gage balance located in the sting. The second series used two six-component balances (Fig. 3) located in the nose and tail sections of the model to measure, independently, the forces and moments acting on the forward (nose) and aft (tail) portions of the fuselage. The absolute angle of attack σ_f could be set at 45°, 60°, 75°, and 90° by selection of the appropriate angle brackets. The nonaxially symmetric fore and aft bodies and the wing could be rolled about the aircraft body x axis to settings of 0°, 5°, and 10°.

Figure 4 illustrates the various components that were tested. As was shown in Fig. 3, each fuselage configuration consisted of a nose section, a circular cylinder center body and a tail section. Nose N_1, a tangent ogive with $\ell/d=3.5$, was chosen to determine how the asymmetric side force exhibited in the static tests by Keener and Chapman[5] was affected by rotation. Nose N_2 consisted of a spherical section blended into a cylinder whose cross-sectional shape was a square with rounded corners. The particular cross-section and corner radius were chosen because the aerodynamic characteristics were known to vary drastically with Reynolds number.[6] The tail configuration T_2 is an approximation of the empennage of a fighter configuration reported[3] to provide an autorotative moment at 90° angle of attack. The wing planform was chosen to coincide with one of the wings of a series of wing-body configurations currently being investigated at the Ames Research Center as part of a general high-angle-of-attack experimental aerodynamics program.

B. Test Conditions

The major portion of the investigation was carried out at nominal unit Reynolds numbers of 2, 6.5, 14, and 20×10^6 m^{-1} (0.6, 2, 4.2, and 6.0×10^6 ft^{-1}) at a Mach number of 0.25. A few selected runs were made at lower Mach numbers, and several runs were made at a Reynolds number of 25×10^6 m^{-1} (7.5×10^6 ft^{-1}) at a Mach number of 0.25. Angles of attack were 45°, 60°, 75°, or 90° and roll angles were 0°, 5°, or 10°. Spin rates were varied from +600 rpm to -600 rpm, which provided reduced spin rates from +0.17 to -0.17.

III. Results and Discussion

A. Configuration N_1T_1

Keener and Chapman[5] reported the existence of a strong side force and yawing moment at high angles of attack and zero sideslip at certain conditions on an $\ell/d=3.5$ tangent ogive nose as well as other forebody shapes. In their work, they reported that the side-force coefficient C_y approached 3.0 between 45° and 60° angle of attack at a Mach number of 0.25 and $R_d=0.8\times10^6$. It was unknown how the asymmetric vortex pattern associated with the side force would be affected by a coning motion. Referring to Fig. 5, which shows the spinning moment coefficient as a function of the normalized spin

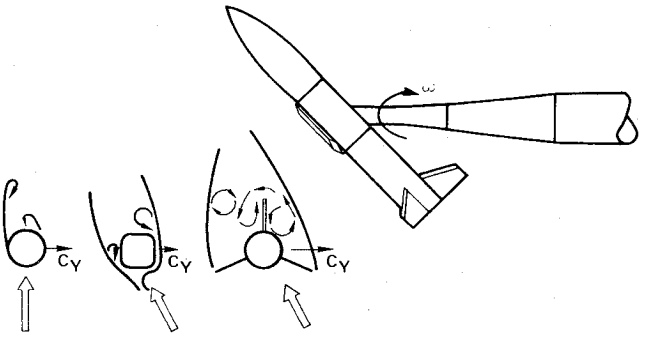

Fig. 1 Sketch of pro-spin flow mechanisms.

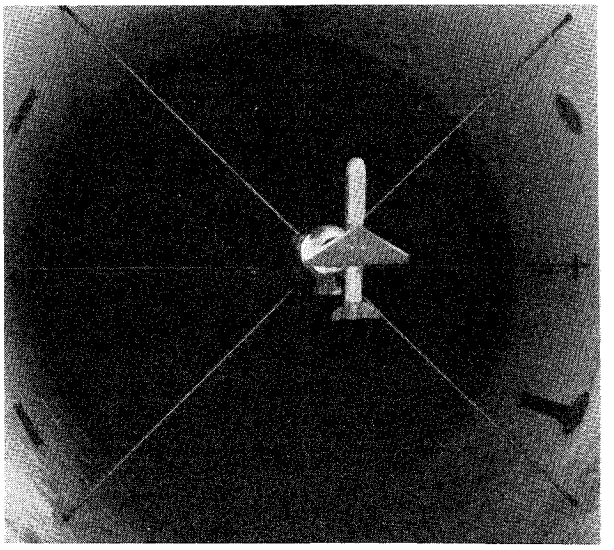

Fig. 2 Photograph of model and rotary apparatus installation in the wind tunnel.

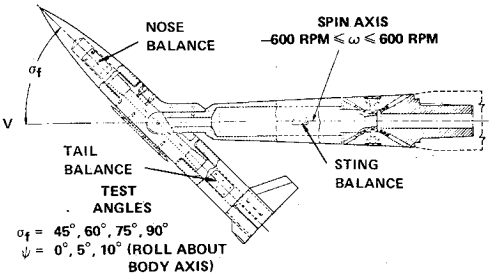

Fig. 3 Sketch of model and balance combinations.

rate Ω(or helix angle) at $\sigma_f=60°$, it would appear that the direction and magnitude of the yaw moment (which contributes to the spinning moment C_R about the sting axis) is not affected greatly by spin rate. The slight negative slope of the curves indicates a small amount of spin damping. It is shown also in Fig. 5 that rotating the nose 90° about its longitudinal axis reversed the sign of C_R. This is not too surprising, since the results in Ref. 5 also showed a change in direction of the forebody side force with rotation of the forebody about the longitudinal axis. In Fig. 6, the side-force coefficient C_y is plotted vs Ω for nose N_1 and tail T_1 at $\sigma_f=45°$. The magnitude of C_y at zero rotation rate for the nose is about the same as that reported in Ref. 5 at the same conditions and does not appear to be affected significantly by spin rate. The magnitude of the side force on the cylindrical tail section is relatively small for all Reynolds numbers. There is, however, a more apparent variation of C_y with Ω at the lowest Reynolds number, which may be partly because of a balance sensitivity problem described in the next section. In summary, it would appear from the nose data that, at least for the conditions and

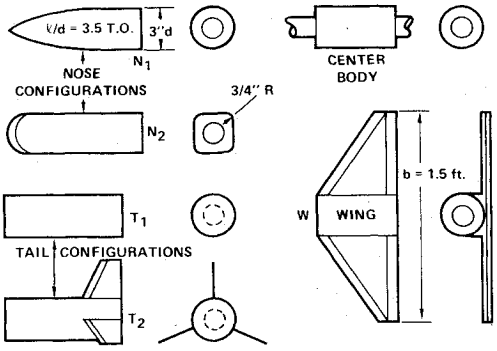

Fig. 4 Sketch of model components.

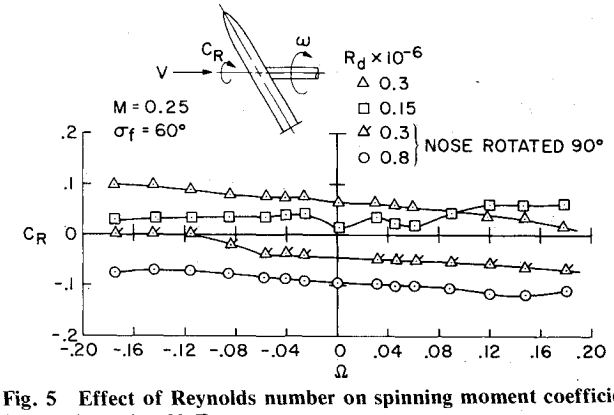

Fig. 5 Effect of Reynolds number on spinning moment coefficient for configuration N_1T_1.

rotation rates shown here, once the asymmetric vortex pattern forms, it "locks into position" and rotates with the model. It must be noted, of course, that to realize an equilibrium spin rate in free rotation a model eventually would have to reach a rotation rate such that the spin moment is equal to zero.

B. Configuration N_2T_1

As mentioned in the Introduction, the square nose section with rounded corners, N_2, was picked because of its known dependence on Reynolds number and because of the availability of the extensive two-dimensional data of Polhamus.[6] Figure 7 shows the comparison of the side-force coefficients obtained at zero rotation rate with the results of Polhamus. Considering that the present model is not completely two-dimensional, the agreement is considered good. The comparison also shows, with hindsight, that it would have been desirable to have defined the transition area better by additional tests, particularly at the lower range of Reynolds numbers. However, this points up a basic problem. In rotary tests, inertial or centrifugal loads on the six-component balance can be quite large, particularly on the normal and axial force gages of the nose and tail balances. This is particularly true for a model designed to be tested at high dynamic pressure requiring high-strength material such as steel, which is also very heavy. Because of time and money restrictions, the present investigation was limited to balances that were already available. Typically, the side-force capacity of those balances is designed for half the normal force capacity. If a balance must be selected to accomodate the high normal inertial loads, then the side-force gages will be ranged too high for the expected aerodynamic side forces. This means a loss in measuring sensitivity. For the lowest Reynolds numbers, the balance sensitivity is marginal and any future testing at low Reynolds numbers to define better this transitional range should be done with more sensitive balances.

The two-dimensional data of Polhamus[6] were used in calculating C_R by employing a simple "blade element" type of analysis. A Reynolds number well below critical and a

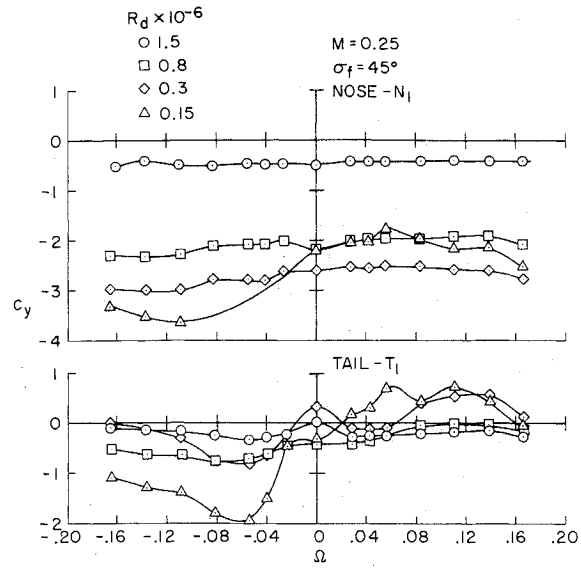

Fig. 6 Effect of Reynolds number on body side-force coefficient for nose and tail sections for configuration N_1T_1.

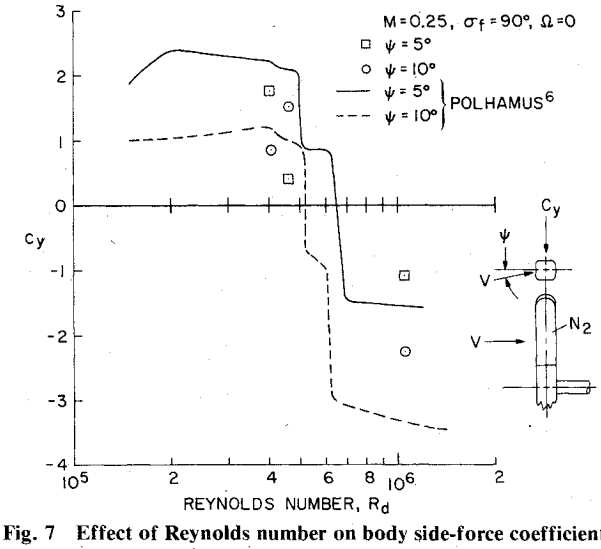

Fig. 7 Effect of Reynolds number on body side-force coefficient for nose N_2 at zero rotation rate.

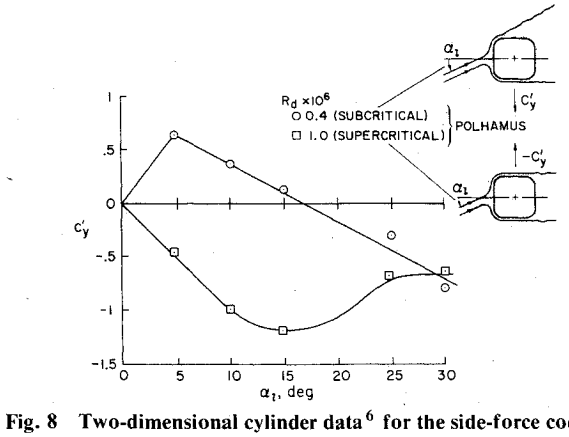

Fig. 8 Two-dimensional cylinder data[6] for the side-force coefficient used in calculation of spin-moment coefficient C_R.

Reynolds number well above critical were chosen to exhibit the two basic types of flow. The variation of the two-dimensional side-force coefficient with angle of attack is shown in Fig. 8 for the two cases of interest. These Reynolds number variations (faired curves) were used to calculate the local side-force coefficient contribution to the spin coefficient

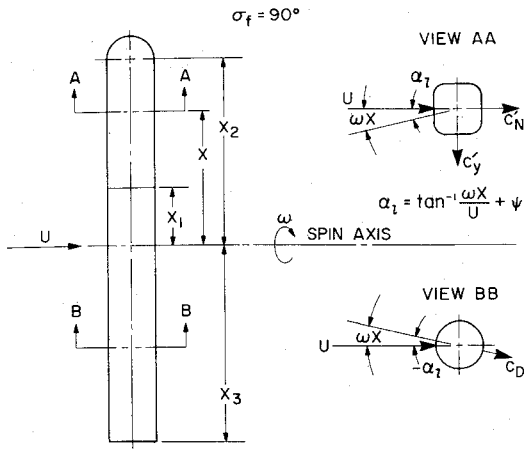

Fig. 9 Sketch of model longitudinal locations and local flow angles used in Eq. (2).

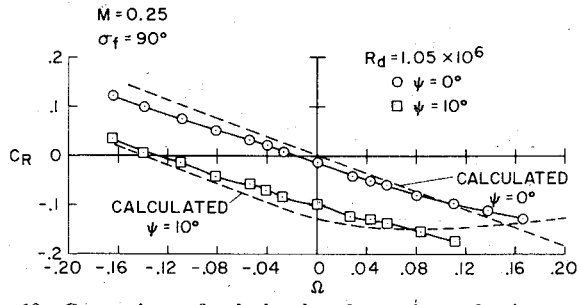

Fig. 10 Comparison of calculated and experimental spin-moment coefficients at supercritical Reynolds numbers for configuration N_2T_1 at $\psi = 0°$ and 10°.

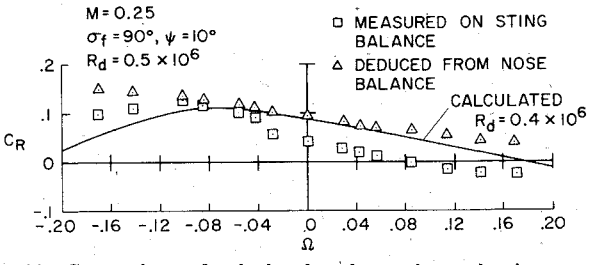

Fig. 11 Comparison of calculated and experimental spin-moment coefficients at subcritical Reynolds numbers for configuration N_2T_1 at $\psi = 10°$.

as shown subsequently. Referring to Fig. 9, which shows a sketch of the model parameters in the calculation, the local angle of attack at a fuselage station which is distance x from the axis of rotation may be expressed by

$$\alpha_l = \tan^{-1}(\omega x/U) + \psi \qquad (1)$$

The maximum value of α_l attained in the investigation occurred at the tip, when $\psi = 10°$ and $\omega = 600$ rpm and was approximately 22.5°. The spinning moment coefficient may be written as

$$C_R = \frac{d}{Sb}\left[\int_{x_3}^{0} c_D \frac{\omega x^2}{U}\,dx - \int_{0}^{x_1} c_D \frac{\omega x^2}{U}\,dx + \int_{x_1}^{x_2} (c_y' \cos\psi + c_N' \sin\psi)x\,dx\right] - C_{D_{\text{sphere}}} \omega x_2^2 \frac{\pi d^2}{8SbU} \qquad (2)$$

where c_y' and c_N' are both functions of α_l, and $x_2 - x_1$ represents the length of the square cross-section nose, which has a constant corner radius. From x_2 to the top is a hemisphere. From the spin axis to x_1 and x_3 the cross section

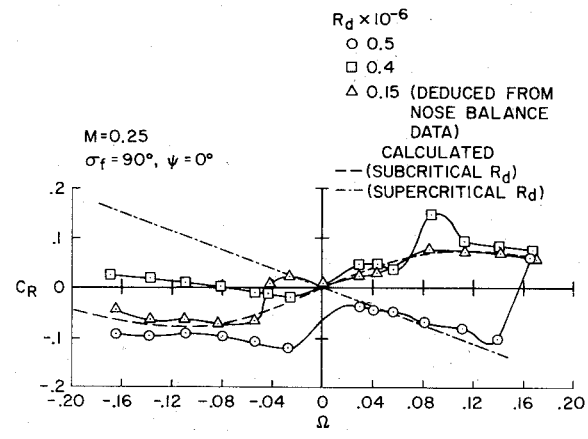

Fig. 12 Comparison of calculated and experimental spin-moment coefficients at Reynolds numbers below and near critical for configuration N_2T_1 at $\psi = 0°$.

is circular. In the first, second, and fourth terms in Eq. (2), $\sin\omega x/U$ has been approximated by $\omega x/U$ and, in each term, the rotational component of velocity has been neglected in the determination of local dynamic pressure.

The term

$$\frac{d}{Sb}\int_{x_1}^{x_2} (c_y' \cos\psi)x\,dx$$

is by far the dominant term in Eq. (2) and, therefore, the curves in Fig. 8 can be used to estimate the behavior to be expected at subcritical and at supercritical Reynolds numbers.

Using Eq. (2) and c_y' from Fig. 8 for the supercritical case, the spin-moment coefficient was calculated for $\sigma_f = 90°$ and body roll angles of $\psi = 0°$ and 10°. These curves are plotted in Fig. 10 along with the measured data points at $R_d = 1.05 \times 10^6$. There is reasonable agreement between experimental and calculated results. Figure 11 shows a similar comparison for the subcritical case at $\sigma_f = 90°$ and $\psi = 10°$. Two sets of data points are shown, one measured directly from the sting balance and the other deduced from forces measured on the nose balance and converted to a spin moment about the rotary sting axis. The agreement is not quite as good as for the supercritical case. Figure 12, where $\sigma_f = 90°$ and $\psi = 0°$, illustrates graphically the problems that can be encountered when testing near the transition range, where the flow is neither clearly subcritical or supercritical. It can be seen that the agreement for the lowest Reynolds number $R_d = 0.15 \times 10^6$ is fairly good, but such is not the case for $R_d = 0.4 \times 10^6$ and 0.5×10^6. In the latter cases, there is a tendency for the flow to change rather unpredictably from one type of flow regime to the other. This tendency also can be observed in Figs. 13 and 14, in particular the forebody curves of N_2T_2 in Figs. 13c and 13d, where the nose side-force coefficient is plotted vs Ω at $R_d = 0.5 \times 10^6$ and in Fig. 14 for both the N_2T_2 and N_2T_2W configurations at $R_d = 0.5 \times 10^6$.

C. Configurations N_2T_2 and N_2T_2W

The behavior of the side-force coefficient for nose N_2 and tail T_2 with Reynolds number is shown in Fig. 13 for $\sigma_f = 45°$, 60°, 75°, and 90°. A side force typical of subcritical flow is exhibited for N_2 for $\sigma_f = 75°$ and 90° (Figs. 13c and 13d) although in an erratic manner. From a simple cross-flow Reynolds number analysis, one would expect subcritical behavior to be more in evidence at the lower values of σ_f, since the cross-flow Reynolds number, based on a decreasing cross-flow velocity component, is decreasing. However, such is not the case, as can be seen from Figs. 13a and 13b, where the data at the lowest Reynolds number actually show more of an antispin behavior than do the data at the larger Reynolds numbers. Apparently, at angles of attack other than 90°, one cannot consider crossflow as the only important component

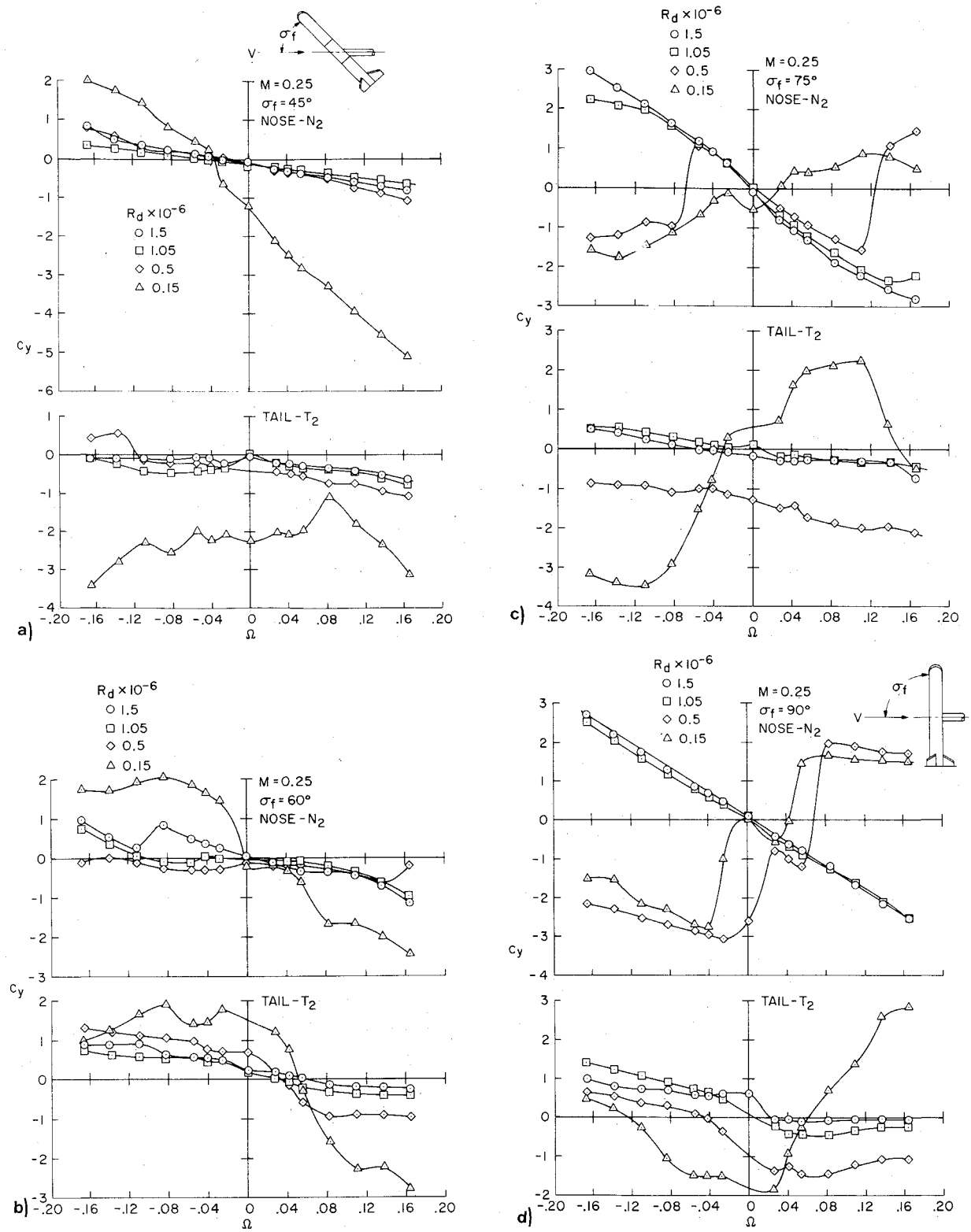

Fig. 13 Effect of Reynolds number on body side-force coefficient for nose and tail sections for configuration N_2T_2; a) $\sigma_f = 45°$, b) $\sigma_f = 60°$ c) $\sigma_f = 75°$, d) $\sigma_f = 90°$

for determining the aerodynamic behavior. The longitudinal flow at angles of attack lower than 90° has a strong influence on the resulting flow pattern around the body.

There is some doubt about the validity of the data on T_2 at the lowest Reynolds number because of the balance sensitivity problem described earlier. For example, the amount of asymmetry in the side-force coefficient with plus and minus Ω at the lowest Reynolds number is surprising and, if correct, certainly raises some interesting questions. In any case, to understand the aerodynamics at lower Reynolds numbers on the present configuration, a balance better suited to the smaller loads should be used. Plans are being considered to conduct further tests on the present configurations.

Results obtained on the sting balance for N_2T_2 and the complete configuration N_2T_2W are shown in Fig. 14 for $\sigma_f = 90°$. Comparing results with and without the wing, the flow remains supercritical at positive Ω but, with the wing, jumps to subcritical at $\Omega \approx 0.06$. Again, at near transitional

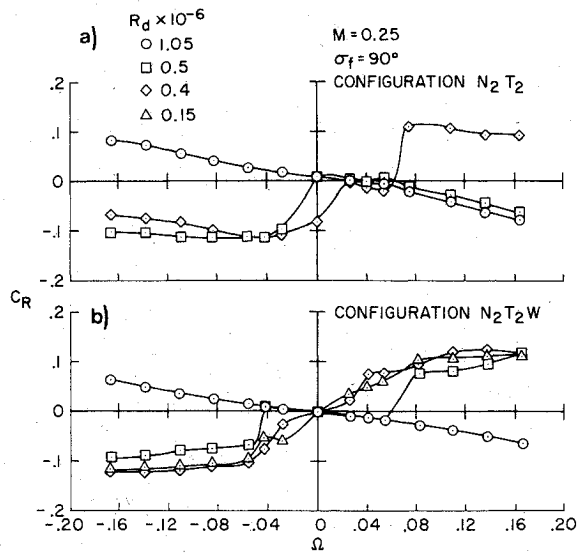

Fig. 14 Comparison of Reynolds number effects for configurations: a) without a wing section, N_2T_2 and b) with a wing section, N_2T_2W.

R_d, the flow can be triggered easily from one condition to another and the wing presence may have been just enough in this case to influence the flow slightly. The strong dependence on Reynolds number of both configurations is shown clearly. For N_2T_2W, a slightly smaller amount of spin damping at the highest Reynolds number indicates that the wing contributes an autorotational moment at that condition. A fairly symmetric variation of C_R with Ω also is evident for N_2T_2W.

IV. Conclusions

Selected results have been presented from exploratory rotary tests made on several airplane-like configurations at high angles of attack in the Ames 12-Ft Pressure Wind Tunnel. These tests show that the rotary coefficients are highly dependent on Reynolds number for the configurations tested. The major effects were found to be as follows:

1) Under conditions where an asymmetric vortex pattern forms on an axially symmetric nose, the pattern appears to "lock in" and rotate with the model.

2) Fuselages with noncircular cross sections which have corner radii are particularly susceptible to variations in Reynolds number. For the particular configuration tested, two-dimensional data used in a simple "blade element" analysis gave reasonable agreement for well-below subcritical and for above critical Reynolds numbers at 90° angle of attack. However, a simple cross-flow analysis was not applicable at angles of attack of 45° and 60°. The results obtained for Reynolds numbers in the transition range were understandably erratic.

3) The characteristics obtained from the tail configuration also varied markedly with Reynolds number and were highly nonlinear with rotational rate. To investigate properly the Reynolds number range near the transition between supercritical and subcritical flow conditions, the model should be retested with a more suitable balance for measuring the forces and moments.

As a general conclusion, it seems clear, as a result of these tests, that aerodynamic coefficients must be measured in the presence of spinning or coning motion if the results are to be applicable to nonstatic cases. Also, when experiments are carried out on a rotary sting apparatus, one must be extremely cautious in applying those measurements to full-scale airplane flight predictions. The effect of Reynolds number should be investigated thoroughly for any configuration tested. In particular, since full-scale Reynolds numbers rarely can be obtained in the wind tunnel, one at least should test in a Reynolds number regime where the results can be extrapolated to full scale with some confidence that the flow conditions are at least similar to the full-scale condition of interest; one should not attempt to apply subcritical test results to a supercritical flight case.

References

[1]Tobak, M. and Schiff, L.B., "Generalized Formulation of Nonlinear Pitch-Yaw-Roll Coupling: Part II–Nonlinear Coning-Rate Dependence," *AIAA Journal*, Vol. 13, March 1975, pp. 327-332.

[2]Bamber, M.J. and Zimmerman, C.H., "The Aerodynamic Forces and Moments Exerted on a Spinning Model of the NY-1 Airplane as Measured by the Spinning Balance," NACA TR 456, 1933.

[3]Chambers, J.R., Bowman, J.S., Jr., and Anglin, E.L., "Analysis of the Flat-Spin Characteristics of a Twin-Jet Swept-Wing Fighter Airplane," NASA TN D-5409, 1969.

[4]Clarkson, M.H., "Autorotation of Fuselages," *AIAA Aeronautical Engineering Review*, Feb. 1958.

[5]Keener, E.R., and Chapman, G.T., "Onset of Aerodynamic Side Forces at Zero Sideslip on Symmetric Forebodies at High Angles of Attack," AIAA Paper 74-770, Anaheim, Calif. 1974.

[6]Polhamus, E.C., "Effect of Flow Incidence and Reynolds Number on Low-Speed Aerodynamic Characteristics of Several Noncircular Cylinders with Applications to Directional Stability and Spinning," NACA TN 4176, Jan. 1958.

[7]Schiff, L.B. and Tobak, M., "Results From a New Wind-Tunnel Apparatus for Studying Coning and Spinning Motions of Bodies of Revolution," *AIAA Journal*, Vol. 8, Nov. 1970, pp. 1953-1957.